Gibbs Topological Analysis for Constructing Phase Diagrams of Binary and Ternary Mixtures

ARTICLE *in* INDUSTRIAL & ENGINEERING CHEMISTRY RESEARCH · NOVEMBER 2002

Impact Factor: 2.59 · DOI: 10.1021/ie020430t

2 AUTHORS, INCLUDING:

Sugata P. Tan
Planetary Science Institute
29 PUBLICATIONS **597** CITATIONS

SEE PROFILE

GENERAL RESEARCH

Gibbs Topological Analysis for Constructing Phase Diagrams of Binary and Ternary Mixtures

Sugata Pikatan Tan and Maciej Radosz*

Department of Chemical and Petroleum Engineering, University of Wyoming, Laramie, Wyoming 82071-3295

A method of mapping and matching the Gibbs energy gradient vectors, referred to as the topological approach, is found to be as reliable and as accurate as the interval method in the tangent-plane phase stability analysis for generating phase diagrams[2] but much more efficient.

Introduction

Phase diagrams, such as $P-T$, $P-xy$, and $T-xy$, are commonly used to illustrate the phase behavior of mixtures. The phase diagrams show phase-boundary curves that represent the conditions of phase transitions. The phase boundaries are usually calculated using a flash method that boils down to solving a set of simultaneous thermodynamic and mass-balance equations. Unfortunately, the flash methods produce solutions that tend to be initial-guess-sensitive, ambiguous, and incomplete: some solutions may be unphysical and some may be missing. The flash user, therefore, needs auxiliary tools for the initialization[1] and for the phase stability analysis. The latter is used to evaluate the flash results and to select the ones that are physically meaningful.

An alternative to such a flash plus phase stability analysis approach to generating phase diagrams is a direct phase stability analysis approach,[2] without a flash-calculation step. In this approach, the phase stability is tested for all of the grid points. Finding two adjacent points of which one is stable and one is unstable is equivalent to finding a phase boundary between them; an interpolation procedure is then used to pinpoint the phase boundary. By scanning the whole phase diagram, one can collect all of the points needed to draw the phase boundaries.

The phase stability probe in this approach is a plane tangent to the Gibbs energy surface at a point of the overall mixture composition.[3] If the tangent plane intersects the Gibbs surface, that is, if there are some points on this plane that lie above the Gibbs surface, the mixture composition is declared to be unstable; the mixture will spontaneously split into different phases.

A prototype of the direct phase stability analysis approach described in our previous paper[2] is on the basis of interval mathematics, originally applied to the tangent-plane method with equations of state (EOSs) or activity coefficient models.[4−6] Such an interval tangent-plane method is framed as a minimization problem. The objective function is the distance from the tangent plane to the Gibbs surface. The interval algorithm guarantees finding a global minimum.[7] If the global minimum is negative, i.e., when the Gibbs surface is below the tangent plane in the vicinity of the minimum, the system is declared to be unstable.

The interval tangent-plane approach to generating phase diagrams described in our previous paper[2] essentially eliminates the problems arising from multiple solution roots and multiple phases and the need for smart initial guesses. However, that approach tends to be CPU-time-intensive, especially when coupled with a complex EOS, such as statistical associating fluid theory (SAFT),[2] and especially when applied to asymmetric mixtures, such as polymer solutions.

Therefore, the goal of this work is to develop a computationally efficient alternative to the interval method for constructing phase diagrams on the basis of the phase stability analysis alone.

Tangent-Plane Method

The objective function in the tangent-plane minimization problem is the distance of the Gibbs energy surface at any overall $\mathbf{x}$ from a plane that is tangent to this Gibbs energy surface at $\mathbf{x} = \mathbf{z}$:

$$D(\mathbf{x},\mathbf{z}) = \tilde{g}^{\mathrm{M}}(\mathbf{x}) - \left[\tilde{g}^{\mathrm{M}}(\mathbf{z}) + \sum_{i=1}^{n}\left(\frac{\partial \tilde{g}^{\mathrm{M}}}{\partial x_i}\right)_{\mathbf{x}=\mathbf{z}}(x_i - z_i)\right] \quad (1)$$

where $\tilde{g}^{\mathrm{M}}$ is the dimensionless molar Gibbs energy of mixing. The bold symbols mean the mole fraction vectors, x_i and z_i mean mole fractions, and n means the number of components. For example, for a binary mixture, where $n = 2$, the mole fraction vector $\mathbf{x}$ consists of two components, x_1 and $x_2 = 1 - x_1$, and so does the feed mole fraction vector $\mathbf{z}$, which consists of z_1 and $z_2 = 1 - z_1$. The partial derivatives with respect to x_i are calculated at $\mathbf{x} = \mathbf{z}$.

To minimize D, the first derivatives of $D(\mathbf{x},\mathbf{z})$ with respect to the mole fractions are set equal to zero:

$$\left(\frac{\partial \tilde{g}^{\mathrm{M}}}{\partial x_i} - \frac{\partial \tilde{g}^{\mathrm{M}}}{\partial x_n}\right) - \left(\frac{\partial \tilde{g}^{\mathrm{M}}}{\partial x_i} - \frac{\partial \tilde{g}^{\mathrm{M}}}{\partial x_n}\right)_{\mathbf{x}=\mathbf{z}} = 0 \qquad i = 1, \ldots, n-1 \quad (2)$$

The roots of eq 2 are the stationary points ($\mathbf{x}^{\mathrm{S}}$): maxima,

* Corresponding author. E-mail: Radosz@uwyo.edu. Tel: 307-766-2500. Fax: 307-766-6777.

10.1021/ie020430t CCC: $22.00
Published on Web 10/15/2002

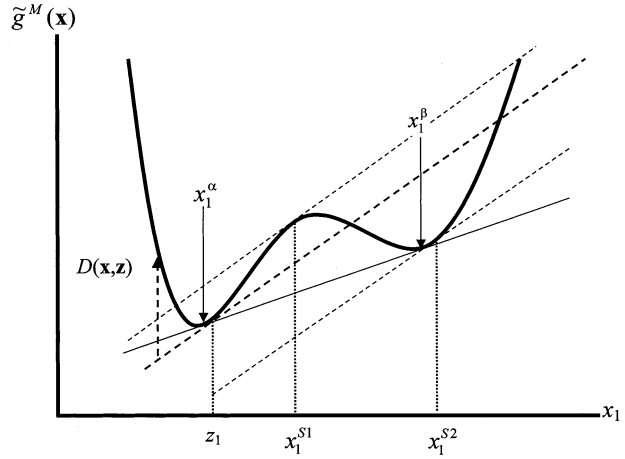

Figure 1. Gibbs energy versus mole fraction for LLE in a binary mixture with Michelsen's tangent lines having the same slope at the stationary points of D according to eq 3.

minima, and inflection points of the function D. We note that $\mathbf{x} = \mathbf{z}$ is a trivial solution of eq 2, which results in $D = 0$. If one can find *all* of the stationary points, which is the case for the interval method described in our previous paper,[2] identifying a global minimum is easy.

Michelsen[8] discovered a very useful property of eq 2, namely, that each stationary point of D must have a tangent plane with the same gradient as that of the tangent plane at $\mathbf{x} = \mathbf{z}$. This means that the directions and corresponding components of the gradient vectors at the stationary points are the same as those of the tangent-plane gradient at $\mathbf{x} = \mathbf{z}$. Figure 1 illustrates Michelsen's finding for a binary mixture, for which eq 2 reduces to a scalar equation as follows:

$$\frac{\mathrm{d}\tilde{g}^{\mathrm{M}}}{\mathrm{d}x_1} = \frac{\partial\tilde{g}^{\mathrm{M}}}{\partial x_1} - \frac{\partial\tilde{g}^{\mathrm{M}}}{\partial x_2} = \left(\frac{\partial\tilde{g}^{\mathrm{M}}}{\partial x_1} - \frac{\partial\tilde{g}^{\mathrm{M}}}{\partial x_2}\right)_{\mathbf{x}=\mathbf{z}} \tag{3}$$

This equation represents the slope of a line that is tangent to the Gibbs energy curve at a given concentration, for example, at the feed concentration z_1 in Figure 1. According to Michelsen's interpretation, the three stationary points of D shown in Figure 1, x_1^{S1}, x_1^{S2}, and the trivial solution at z_1, will have tangent lines of the same gradient; all of these tangent lines are shown as dashed lines in Figure 1. The qualitative example in Figure 1 shows a minimum of D at x_1^{S2} and a local maximum at x_1^{S1}. The global minimum clearly is at x_1^{S2}. Because this global minimum is negative (below the tangent line), one concludes that feed z_1 is unstable, and hence it will split into two phases having compositions of x_1^α and x_1^β. These compositions are determined from a common tangent line of the two troughs of the Gibbs energy (solid line in Figure 1). In fact, any feed that falls between x_1^α and x_1^β will split into two phases having compositions of x_1^α and x_1^β.

For ternaries, there are two components of the gradient vector of the Gibbs surface: one along the x_1 axis (unit vector $\hat{\imath}$) and one along the x_2 axis (unit vector $\hat{\jmath}$).

$$\nabla\tilde{g}^{\mathrm{M}} = \left(\frac{\partial\tilde{g}^{\mathrm{M}}}{\partial x_1} - \frac{\partial\tilde{g}^{\mathrm{M}}}{\partial x_3}\right)\hat{\imath} + \left(\frac{\partial\tilde{g}^{\mathrm{M}}}{\partial x_2} - \frac{\partial\tilde{g}^{\mathrm{M}}}{\partial x_3}\right)\hat{\jmath} \tag{4}$$

At the stationary points of D, both components of the vector are equal to their counterparts at $\mathbf{x} = \mathbf{z}$; thus, eq 2 will result in two equations corresponding to the two gradient vector components. For mixtures with n components, eq 2 will result in $n - 1$ equations corresponding to the $n - 1$ gradient vector components.

There is another useful application of eq 2. Suppose we are to test the phase stability of a point that happens to be *on* a phase boundary, that is, a point that coincides with an equilibrium phase composition, say at x_1^α in Figure 1. Then, as z_1 shifts toward x_1^α in Figure 1, the three parallel tangent lines shown as dashed lines shift and rotate until two of them merge when $z_1 = x_1^\alpha$ to form a single tangent line shown as a solid line in Figure 1, which we refer to as a tie line. Such a tie line is tangent to the Gibbs surface at both equilibrium compositions x_1^α and x_1^β. In other words, the two stationary points calculated from eq 2, i.e., z_1 (trivial solution) and x_1^{S2} (nontrivial solution), now coincide with the equilibrium phase compositions: x_1^α and x_1^β, respectively. Consequently, these two stationary points have the same D value, i.e., $D = 0$.

The phase stability test on each reference phase-boundary point, therefore, produces a set of stationary points having D values equal to zero: a trivial solution corresponding to the reference point being tested and some nontrivial solutions (at least one). The reference point and the other stationary points in the set represent the compositions of all of the phases coexisting in a state of equilibrium. In this work, we refer to this approach as the tie-line approach and use it to estimate a three-phase equilibrium and to draw tie lines in phase diagrams.

Constructing the Phase Diagram

Michelsen's interpretation of eq 2, which allows for an efficient search of the stationary points of D, suggests a direct topological approach to the tangent-plane minimization problem. This approach is different, in either mathematical or computational detail, from that of Wasylkiewicz et al.,[9] who used the Hessian of D to help track the ridges and valleys of D in search of the stationary points; their approach applies to liquid−liquid equilibrium (LLE) only.

A direct topological approach to generating a phase diagram used in this work consists of the following steps:

(1) Testing phase stability at $\mathbf{x} = \mathbf{z}$ at P and T.

(a) Dividing the whole composition space into a collection of grid points.

(b) Calculating the gradient vector of the Gibbs surface at each grid point as the reference (gradient mapping).

(c) Searching for all gradient vectors from the reference map that match the gradient vector at a composition of interest $\mathbf{x} = \mathbf{z}$ (gradient matching). Because of the discrete nature of the map, an interpolation procedure is needed to do the exact matching.

(d) Selecting the global minimum and testing for stability at $\mathbf{z}$ (a negative global minimum means instability; positive means stability).

(2) Plotting the phase diagram.

(a) Systematically testing phase stability at each $\mathbf{z}$ (for $P-xy$ or $T-xy$) or P or T (for $P-T$) in the range of interest, throughout the phase diagram, which means repeating steps 1a−d for each $\mathbf{z}$ or P or T. For $P-xy$ and $T-xy$ diagrams, the mapping step can be done only once for each P and T pair.

(b) Searching for all of the pairs of points in the phase diagram that exhibit a stable-to-unstable transition (boundary search).

(c) Interpolating to pinpoint the exact location of the phase boundary.

(d) Plotting the phase diagram.

In the gradient-mapping step, which is the most time-consuming step, the overall efficiency and accuracy depend on the choice of the grid; the smaller the grid size, the lower the efficiency but the higher the accuracy. We have two options to increase the accuracy: one is to use a single interpolation over the map with a finer grid size, and the other is to use successive focusing interpolation cycles over the map with a coarser grid size. The single interpolation is faster for constructing phase diagrams at constant P and T because the gradient mapping is done only once. The focusing interpolation is faster for constructing $P-T$ diagrams where the gradient mapping is done many times; it is turned on when a unit containing the desired result is found (then such a unit is subdivided into smaller units). Unless stated otherwise, the phase stability tests in this work are carried out using the single interpolation.

While the number of the grid points, and hence the grid size, is the main factor of the accuracy, the method of matching also plays a role. In general, we use linear interpolation for binaries and bilinear interpolation for ternaries. For more complex mixtures, one may need a higher order interpolation method. In the examples below, we use the linear and bilinear interpolation, described in detail in Appendix A.

For asymmetric mixtures (where components substantially differ in molecular weight), one needs a smaller grid size throughout and a logarithmic scale at low concentrations of the large component. A useful rule of thumb is to start with a grid size of $\Delta x = 0.01$ for symmetric systems. For moderately asymmetric systems, the grid size can be reduced to 0.005, and for strongly asymmetric systems, such as polymer solutions, it can be further reduced to 0.001.

If it happens during the mapping that there is more than one density available at a certain composition, one takes the density with the lowest Gibbs energy.

Examples and Working EOS

Examples used in this work are the same as those used to illustrate the interval method:[2] polyethylene NIST 1483 (1)/ethylene (2), *n*-tetracontane (1)/propane (2), and ethane (1)/heptane (2)/butane (3) and an additional example of a phase stability test for H_2S (1)/CH_4 (2). This additional example is taken from Michelsen[8] and is used here because it is considered[4,8,10,11] to be a difficult phase stability problem. Phase stability tests on three points for the polyethylene (1)/ethylene (2) system are referred to the experimental and modeling work of Chan et al.[12] The $P-xy$ diagram of the *n*-tetracontane (1)/propane (2) system is referred to the experimental cloud-point data taken by Luszczyk and Radosz.[13] The triangular diagram of the ternary system is referred to the experimental data taken by Blas and Vega.[14] Unless stated otherwise, all compositions are given in weight fractions.

The working EOS for the H_2S (1)/CH_4 (2) system is the Soave−Redlich−Kwong (SRK) EOS. The working EOS for the other systems is SAFT,[15,16] for which the dimensionless Gibbs energy of mixing is as follows:

$$\tilde{g}^{M}(\mathbf{x}) = \tilde{a}^{res}(\mathbf{x}) + Z(\mathbf{x}) - \ln v(\mathbf{x}) - \sum_{i=1}^{n} x_i(\tilde{a}_i^{res} + Z_i - \ln x_i v_i) \quad (5)$$

where $v(\mathbf{x})$ is the mixture molar volume, $Z(\mathbf{x})$ is the mixture compressibility factor, Z_i is the compressibility factor for pure component i, v_i is the molar volume for pure component i, $\tilde{a}^{res}$ is the dimensionless residual Helmholtz energy for the mixture, and $\tilde{a}_i^{res}$ is the dimensionless residual Helmholtz energy for pure component i.

The SRK parameters are taken from Hua et al.[4] The SAFT parameters for each component are taken from Huang and Radosz,[15] except for the polymer (with number-average molecular weight $M_n = 28\,900$) and *n*-tetracontane, which is taken from Chan et al.,[12,17] respectively. The binary interaction parameters, k_{ij}, are set equal to zero, except for SRK EOS and for polyethylene NIST 1483 (1)/ethylene (2), for which the temperature-dependent k_{ij} is taken from Chan et al.[12] All SRK and SAFT parameters used in this work are given in Appendix B.

Results and Discussion

The first two examples illustrating the phase stability analysis are for the H_2S (1)/CH_4 (2) system at $P = 40.53$ bar and $T = 190$ K, with feed mole fractions of $z_1 = 0.0115$, $z_1 = 0.0187$, and $z_1 = 0.89$, and for the polyethylene NIST 1483 (1)/ethylene (2) system at $T = 433.15$ K at $P = 1465$ bar, with weight fractions $z_1 = 0.14$ and 0.15, and at $P = 1455$ bar, with $z_1 = 0.15$.

The results for H_2S (1)/CH_4 (2) using the single interpolation method over a grid size of 0.01 are given in Table 1. They are consistent with those obtained by Hua et al.,[4] except for their two stationary points for $z_1 = 0.0115$, one stationary point for $z_1 = 0.0187$, and one stationary point for $z_1 = 0.89$, which are missing. These local minima obtained for unphysical densities from the interval method, and shown in Table 1, are correctly absent from the topological results. The missing local minima fall in the region of unphysical densities (dashed lines in Figure 2). Such stationary points are eliminated in the topological approach when the densities other than the one with the lowest Gibbs energy are rejected in the mapping step of the algorithm.

An overview of the topological results in Table 1 reveals that the accuracy can be improved; such inaccurate trivial solutions signal a need for improvement. As described before, we have two options to improve the accuracy. If we choose a finer grid size, for example, 0.0025, we reproduce the results of the interval method. If we choose the successive interpolations, we obtain the same results 2 times faster (0.016 s versus 0.032 s on Pentium 4, 1.8 GHz).

The results of the phase stability test for NIST 1483 (1)/ethylene (2) obtained from the topological approach are given in Table 2. The corresponding stationary points of D are shown in Figure 3; the stationary point numbers 3 are at $\mathbf{x} = \mathbf{z}$ and hence are the trivial solutions. With a mapping grid size $\Delta x_1 = 0.001$, the topological method takes 2 orders of magnitude less CPU time than the interval method does, while the results are identical. This will make a drastic difference in generating phase diagrams for polymeric systems.

The next example illustrates constructing a $P-xy$ diagram for *n*-tetracontane (1)/ propane (2) at $T = 365$

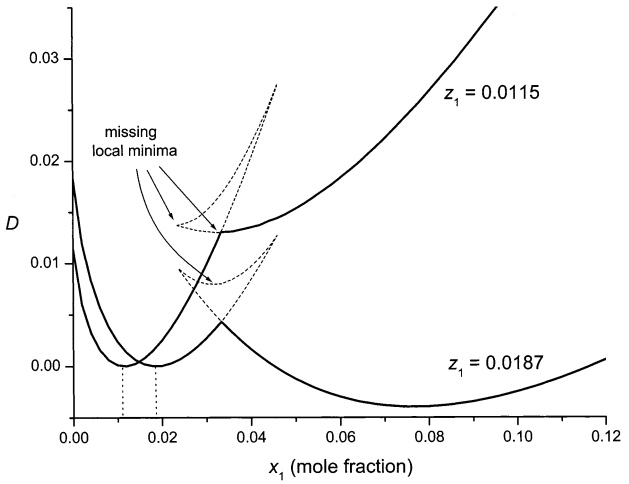

Figure 2. $D-x$ diagram for H_2S (1)/CH_4 (2) at $P = 40.53$ bar and $T = 190$ K for mole fractions $z_1 = 0.0115$ and $z_1 = 0.0187$ at the vicinity of missing stationary points.

Table 1. Comparison of Stationary Points (x_1^S) Obtained from the Topological Method in a Single Interpolation (Map Grid Size 0.01) with Those Obtained from the Interval Method[4] for H_2S (1)/CH_4 (2) at $P = 40.53$ bar and $T = 190$ K

	topological method		interval method[4]	
z_1	x_1^S (mol)	$D(\mathbf{x}^S)$	x_1^S (mol)	$D(\mathbf{x}^S)$
0.0115	0.0120	1.2×10^{-6}	0.0115	0
			0.0237	0.0137
			0.0326	0.0130
0.0187	0.0190	3×10^{-6}	0.0187	0
	0.0769	−0.004	0.7670	−0.004
	0.4905	0.0730	0.4905	0.0729
	0.8846	0.0109	0.8848	0.0109
			0.0313	0.0079
0.89	0.0194	0.0111	0.0192	0.0113
	0.0809	0.0056	0.0809	0.0058
	0.4726	0.0723	0.4726	0.0724
	0.89	0	0.89	0
			0.0319	0.0189

Table 2. Stationary Points (x_1^S) Obtained from the Topological Method in a Single Interpolation (Map Grid Size 0.001) for NIST 1483 (1)/Ethylene (2) at $T = 433.15$ K

			CPU time[a] (s)	
z_1	x_1^S	$D(\mathbf{x}^S)$	topological method	interval method[2]
0.15, $P = 1455$ bar	0.0225	-3.13×10^{-6}	0.06 + 11.81	1387
	0.0889	3.36×10^{-6}		
	0.1500	0		
0.15, $P = 1465$ bar	0.0284	2.65×10^{-6}	0.05 + 11.33	1374
	0.0764	5.17×10^{-6}		
	0.1500	0		
0.14, $P = 1465$ bar	0.0248	-3.73×10^{-6}	0.05 + 11.33	1461
	0.0908	1.64×10^{-6}		
	0.1400	0		

[a] CPU time for Intel Pentium 4, 1.8 GHz; for the topological method, the matching and mapping times are shown.

K and $P = 36.475$ bar. Being faced with a relatively large difference in the molecular weight (although not as large as in the previous example) and anticipating the presence of the vapor phase at low *n*-tetracontane concentrations, we use a smaller grid size, $\Delta x_1 = 0.005$, and a logarithmic scale for dilute concentrations of the heaviest component, between $x_1 = 10^{-10}$ and 10^{-3}. The gradient mapping results are presented in Figure 4, with an inset of the region $x_1 < \Delta x_1$ in a logarithmic scale. The gradient is found to have a discontinuity at

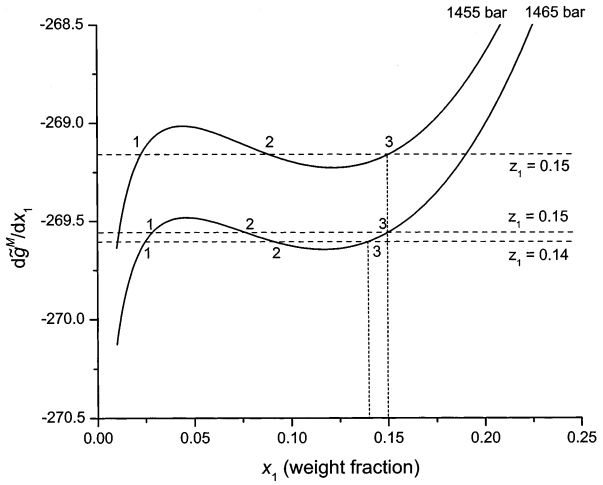

Figure 3. Gradient of the Gibbs energy for NIST 1483 (1)/ethylene (2) at $T = 433.15$ K. Points with number (1, 2, 3) are the stationary points of D.

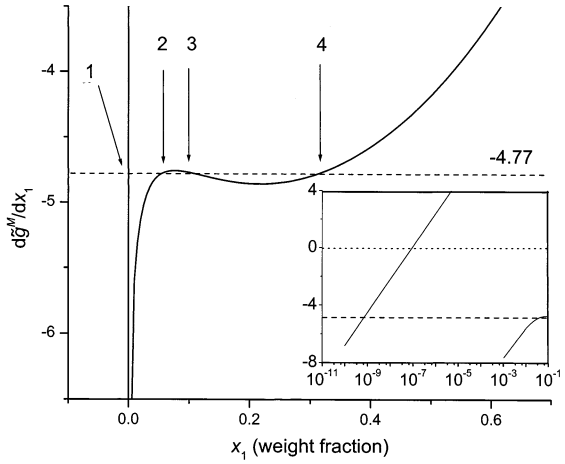

Figure 4. Gradient of the Gibbs energy for *n*-tetracontane (1)/propane (2) at $P = 36.475$ K and $T = 365$ K. The horizontal dashed line at −4.77 is the gradient at $z_1 = 0.06$.

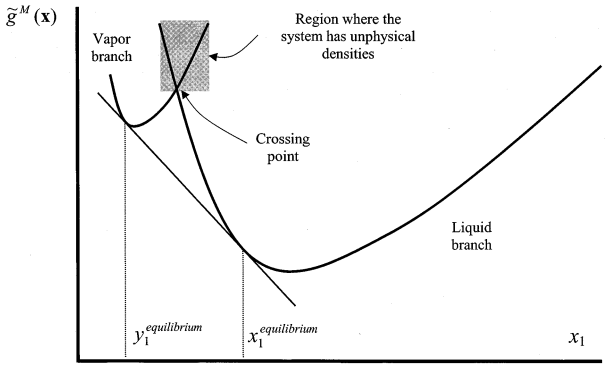

Figure 5. Vapor and liquid branches of the Gibbs energy for a typical binary VLE system.

about $x_1 = 1.04 \times 10^{-3}$ (8.15×10^{-5} in mole fraction), from positive to negative along the x_1 axis, as shown in the inset. Such a change of the gradient sign is due to a crossing between two branches of the Gibbs energy shown in Figure 5 for a typical binary vapor−liquid equilibrium (VLE) system. The Gibbs energy gradient shown in Figure 5 is discontinuous and changes sign from positive to negative at the point where the two branches for vapor and liquid have a crossing point.

Table 3. Comparison of Stationary Points (x_1^S) Obtained from the Topological Method in a Single Interpolation (Map Grid Size 0.005) with Those Obtained from the Interval Method[2] for *n*-Tetracontane (1)/Propane (2) at P = 36.475 bar, T = 365 K, and z_1 = 0.02 and 0.06 (Weight Fractions)

	topological method			interval method[2]		
	x_1^S (mol)	$D(\mathbf{x}^S)$	CPU time[a] (s)	x_1^S (mol)	$D(\mathbf{x}^S)$	CPU time[a] (s)
0.02	4.1523×10^{-11}	-1.8109×10^{-4}	0.55 + 15.25	4.1523×10^{-11}	-1.8109×10^{-4}	17.92
	1.5956×10^{-3}	0		1.5956×10^{-3}	0	
				1.6915×10^{-7}	2.1448×10^{-2}	
0.06	6.0163×10^{-11}	7.7683×10^{-4}	0.45 + 15.25	6.0163×10^{-11}	7.7683×10^{-4}	53.97
	4.9737×10^{-3}	0		4.9737×10^{-3}	0	
	8.4539×10^{-3}	2.6927×10^{-5}		8.4629×10^{-3}	2.6928×10^{-5}	
	3.5400×10^{-2}	-1.5074×10^{-3}		3.5402×10^{-2}	-1.5074×10^{-3}	
				2.4506×10^{-7}	2.2406×10^{-2}	

[a] CPU time for Intel Pentium 4, 1.8 GHz; for the topological method, the matching and mapping times are shown.

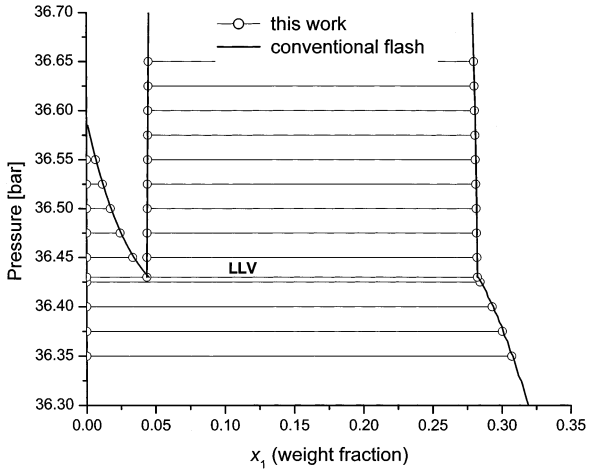

Figure 6. $P-xy$ diagram for *n*-tetracontane (1)/propane (2) at T = 365 K.

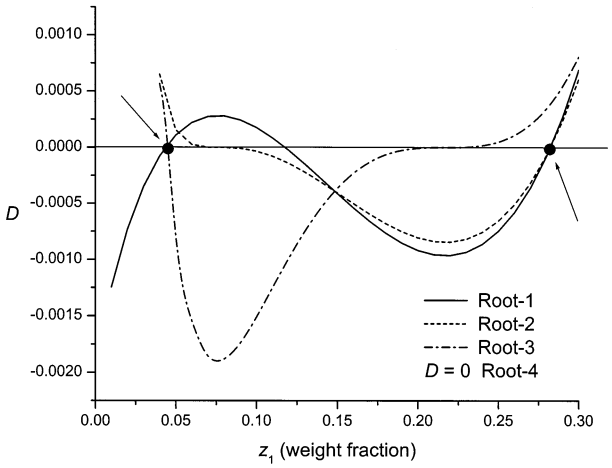

Figure 7. $D-z$ diagram for *n*-tetracontane (1)/propane (2) at T = 365 K and P = 36.43 bar. Root 4 (D = 0) is the trivial root.

The CPU time needed for the mapping step is 15.25 s. The gradient matching for weight fraction $z_1 = 0.02$ gives two stationary points and the gradient matching for $z_1 = 0.06$ gives four stationary points, which are compared in Table 3 with those obtained from the interval method.[2] The agreement is almost perfect. As in our example of H_2S/CH_4, local minima corresponding to unphysical densities are correctly missing in Table 3. In our previous paper,[2] such a stationary point (second root in Figure 6 in the paper) is never a global minimum and always has a positive D value. The shaded area in Figure 5 highlights the mole fraction range of the unphysical densities. For $z_1 = 0.06$, having the gradient of -4.77, the four stationary points given by the topological method in Table 3 (in mole fractions) are pointed by arrows in Figure 4. The corresponding weight fractions of these points are $x_1 = 7.68 \times 10^{-10}$, 0.060, 0.098, and 0.319.

To construct a $P-xy$ diagram, at any given pressure, we do the mapping and matching with a step size of $\Delta x_1 = 0.01$ for the whole composition range and then repeat it for other pressures. In each step, we test the composition for phase stability. When we cross a phase boundary, that is, when we detect a stable-to-unstable transition, or vice versa, we use an interpolation routine to pinpoint the phase boundary, as we did before.[2] At P = 36.475 bar the phase boundaries are found to be exactly the same as those calculated using the interval method, i.e., $x_1 = 0.0244$, 0.0439, and 0.2819.

At P = 36.475 bar, the CPU time needed for the mapping and matching for 100 points ($x_1 = 0-1$) is 42.48 s, including the 27.23 s for the matching alone. For comparison, the interval analysis takes 59 min 43 s to do the same job, which is more than 80 times longer.

As a matter of fact, the topological method can be made even more efficient because the two boundaries, 0.0439 and 0.2819, can be obtained simultaneously using the tie-line approach described earlier. While testing the phase stability at $z_1 = 0.0439$, we find a nontrivial stationary point of 0.2819 which has the lowest D value. The D value at 0.2819 should be zero, as it is for 0.0439, but, as a result of the discrete calculation, this is a small number instead. These two boundaries bracket an unstable region, equivalent to 23 steps with a size of 0.01. Therefore, a subroutine can be added to skip these 23 steps and save time (about 6 s). While testing the phase stability at $z_1 = 0.0244$, we can find another boundary, namely, $x_1 = 5.9 \times 10^{-10}$, which essentially coincides with zero.

Figure 6 shows a $P-xy$ diagram from 36.35 to 36.65 bar, including tie lines. The regions with the tie lines are unstable, two-phase regions. The tie line ends indicate the equilibrium compositions. A vapor−liquid−liquid tie line is found at P = 36.43 bar; its phase stability analysis is shown in Figure 7. Utilizing the tie-line approach described earlier, we find three stationary points (roots of eq 2) having D = 0 when testing the phase stability of the phase-boundary points $z_1 = 0.0437$ and $z_1 = 0.2824$ (pointed by arrows in Figure 7). These stationary points are roots 1, 3, and 4 (trivial root) at $z_1 = 0.0437$ and roots 1, 2, and 4 (trivial root) at $z_1 = 0.2824$. These roots are the compositions of the three coexisting equilibrium phases: $x_1 = 7.1 \times 10^{-10}$, 0.0437, and 0.2824 for vapor, propane-rich liquid, and tetracontane-rich liquid, respectively.

Table 4. Comparison of Stationary Points (x_1^S/x_2^S) Obtained from the Topological Method in a Single Interpolation (Map Grid Size 0.01) with Those Obtained from the Interval Algorithm[2] for Ethane (1)/Heptane (2)/Butane (3) at T = 394.26 K and P = 48.26 bar, and z_1/z_2 (mol) = 0.9/0.04 and 0.6/0.2

	topological method			interval method[2]		
z_1/z_2 (mol)	x_1^S/x_2^S (mol)	$D(\mathbf{x}^0)$	CPU time[a] (s)	x_1^S/x_2^S (mol)	$D(\mathbf{x}^0)$	CPU time[a] (s)
0.90/0.04	0.5506/0.3434	0.1094	0.27 + 355.73	0.5507/0.3435	0.1094	193.28
	0.7027/0.1984	0.1383		0.7027/0.1921	0.1391	
	0.9/0.04	0		0.9/0.04	0	
0.6/0.2	0.8618/0.0273	−0.1552	0.23 + 355.73	0.8624/0.0269	−0.1552	563.44
	0.6362/0.1695	0.0005		0.6366/0.1693	0.0005	
	0.6/0.2	0		0.6/0.2	0	

[a] CPU time for Intel Pentium 4, 1.8 GHz; for the topological method, the matching (short) and mapping (long) times are shown.

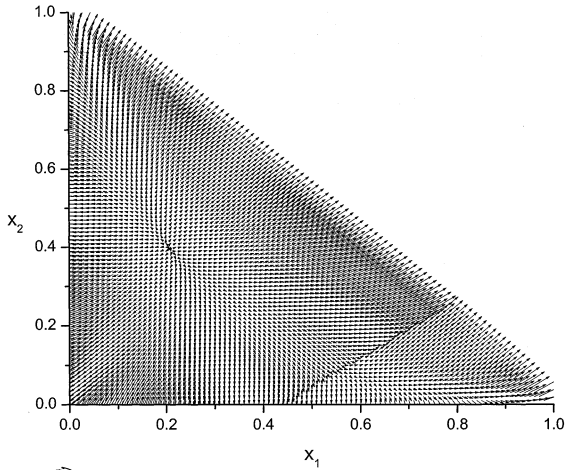

Figure 8. Gradient of the Gibbs energy for ethane (1)/heptane (2)/butane (3) at T = 394.26 K and P = 48.26 bar.

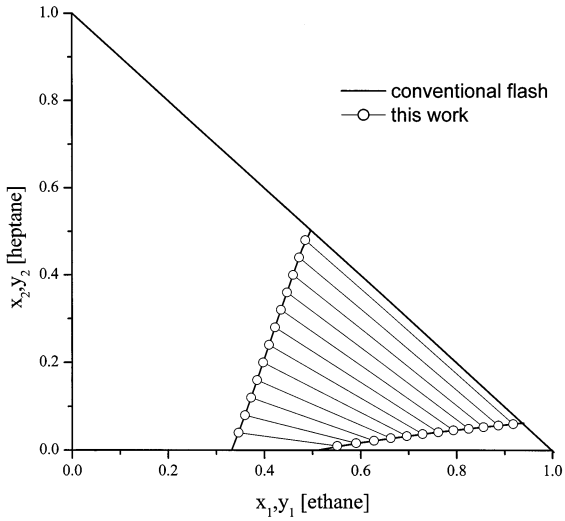

Figure 9. Phase diagram of ethane (1)/heptane (2)/butane (3) at T = 394.26 K and P = 48.26 bar.

The last example is ethane (1)/heptane (2)/butane (3) at T = 394.26 K and P = 48.26 bar. The gradient map has a grid size of $\Delta x_1 = \Delta x_2 = 0.01$. Figure 8 shows the gradient map with a reduced number of grids for clarity. A discontinuity observed near the lower right corner tells us that the Gibbs surface has two branches corresponding to two different phases, vapor and liquid. This observation can also be explained with the Gibbs energy crossing for the vapor and liquid, which is similar to that for a binary system shown in Figure 5.

The gradient matching for mole fractions z_1/z_2 = 0.9/0.04 and 0.6/0.2 gives three stationary points each, which are compared in Table 4 with those calculated by the interval method. The agreement is excellent.

To construct the phase diagram in Figure 9, we use the step size of $\Delta x_1 = \Delta x_2 = 0.01$, which means 4950 composition points to be tested for phase stability (points with $x_1 = 0$, $x_2 = 0$, and $x_3 = 0$ are not tested), and hence 4950 gradient matching cycles. The gradient mapping alone takes 356 s. More than 5000 gradient matching cycles (including those in the interpolation cycles to find the exact phase boundaries), approximately lasting 0.2 s each, take about 24 min throughout the composition space. The total time for the diagram construction is then 6 + 24 = 30 min. By contrast, constructing such a phase diagram using the interval method takes much longer time because *each* phase diagram point may take as long as 193 s or much longer (as shown in Table 4). For testing the 4950 points, the interval method would take about 1 week's time, which is about 300 times longer.

At a given mole fraction x_2, say x_2 = 0.04, there are 95 points to test. The phase boundaries found this way essentially coincide (to within 0.0001) with those calculated using the interval method:[2] x_1 = 0.3459 and 0.7524. The corresponding equilibrium compositions for the other phases are also found using the tie-line approach. For example, we find an equilibrium composition of x_1/x_2 = 0.4186/0.2685 for the 0.7524/0.04 boundary case. Using a conventional flash routine for a feed of z_1/z_2 = 0.5855/0.1543, which is the midpoint of the tie line between those two points, we obtain the same result. The tie lines shown in Figure 9 were all obtained from the phase stability tests on the left phase boundary alone. The CPU time needed for testing these 95 points at x_2 = 0.04 is 6 min 22 s, including only about 26 s for matching alone. The interval method takes 223 min to do the same job, which is about 35 times longer.

Conclusion

A method of mapping and matching the Gibbs energy gradient vectors, referred to as the topological approach to the tangent-plane stability analysis for generating phase diagrams, is found to be as reliable and as accurate as the interval method but much more efficient. For a polymer solution, such as that in our first example, the topological approach takes a factor of 100 less CPU time than the interval method does for the phase stability tests. For constructing phase diagrams, similar to our binary and ternary examples, the time can be reduced by as much as 300 times (ternary mixture).

Acknowledgment

This work is funded by NSF Grant CTS-9908610.

Appendix A. Interpolation Method

The gradient matching for binaries is on the basis of linear interpolation of values ϕ_i (at x_1^i) and ϕ_{i+1} (at x_1^{i+1}) at a point x_1^0 ($x_1^i < x_1^0 < x_1^{i+1}$), which leads to

$$\phi_0 = \frac{(x_1^{i+1} - x_1^0)\phi_i + (x_1^0 - x_1^i)\phi_{i+1}}{x_1^{i+1} - x_1^i} \tag{A1}$$

where i is the grid number. When ϕ_0 is known, x_1^0 can be easily calculated. When a logarithmic scale is used, the interpolation is done over the logarithmic scale by replacing x_1 by $\log x_1$.

The gradient matching for ternaries is on the basis of bilinear interpolation. The interpolation surface unit is a rectangle or a square with vertexes (x_1^i, x_2^i), (x_1^{i+1}, x_2^i), (x_1^{i+1}, x_2^{i+1}), and (x_1^i, x_2^{i+1}), except near the line $x_1 + x_2 = 1$, where the interpolation surface unit is a triangle. Using a common formula of bilinear interpolation,[18] the vector components (v_k^0 with $k = 1$ and 2) at a point (x_1^0, x_2^0) inside the surface unit are

$$v_k^0 = (1-t)(1-u)v_k^{i,i} + t(1-u)v_k^{i+1,i} + tuv_k^{i+1,i+1} + (1-t)uv_k^{i,i+1} \tag{A2}$$

where $v_k^{i,j}$ is the vector component at point (x_i, y_j), and

$$t = \frac{x_1^0 - x_1^i}{x_1^{i+1} - x_1^i} \tag{A3}$$

$$u = \frac{x_2^0 - x_2^i}{x_2^{i+1} - x_2^i} \tag{A4}$$

For a known gradient vector, two equations from eq A2 for each vector component will give us the position of the vector: (x_1^0, x_2^0). At regions near the line $x_1 + x_2 = 1$, where the surface unit is a triangle, the interpolation is similar but with three vertexes instead of four.

In matching the gradients, one needs to predict which surface units contain the expected values, so that the interpolation is carried out only for these units. Such a unit selection takes advantage of the fact that

$$\min_{i,j} v_k^{i,j} \le v_k^0 \le \max_{i,j} v_k^{i,j} \tag{A5}$$

in a sufficiently small surface unit. There are some units satisfying eq A5 for a particular stationary point (x_1^0, x_2^0). The true unit containing (x_1^0, x_2^0) must satisfy a second criterion deduced from eqs A3 and A4:

$$0 \le t \le 1; \quad 0 \le u \le 1 \tag{A6}$$

Appendix B. EOS Parameters Used in the Examples

SRK for H_2S (1)/CH_4 (2):[4]
$P_{c1} = 89.4$ bar, $T_{c1} = 373.2$ K, $\omega_1 = 0.1$, $P_{c2} = 46$ bar, $T_{c2} = 190.6$ K, $\omega_2 = 0.008$, $k_{12} = 0.08$

SAFT for NIST 1483 (1)/ethylene (2):[12]
$m_1 = 1348.8$, $u_{01}/\kappa = 210.0$, $v_{001} = 12.0$, $m_2 = 1.464$, $u_{02}/\kappa = 212.06$, $v_{002} = 18.157$, $k_{12} = 0.067$ (at $T = 433.15$ K)

SAFT for *n*-tetracontane (1)/propane (2):[17]
$m_1 = 26.971$, $u_{01}/\kappa = 210.0$, $v_{001} = 11.963$, $m_2 = 2.696$, $u_{02}/\kappa = 193.0$, $v_{002} = 13.457$

SAFT for ethane (1)/heptane (2)/butane (3):[15]
$m_1 = 1.941$, $u_{01}/\kappa = 191.44$, $v_{001} = 14.460$, $m_2 = 5.391$, $u_{02}/\kappa = 204.61$, $v_{002} = 12.282$, $m_3 = 3.458$, $u_{03}/\kappa = 195.11$, $v_{003} = 12.599$

List of Symbols

$\tilde{a}^{res}(\mathbf{x})$ = dimensionless residual Helmholtz energy of mixture at composition $\mathbf{x}$
$\tilde{a}_i^{res}$ = dimensionless residual Helmholtz energy of pure component i
$D(\mathbf{x},\mathbf{z})$ = distance of the Gibbs energy surface from the tangent plane passing through a particular feed $\mathbf{z}$ at composition $\mathbf{x}$
$\tilde{g}^M(\mathbf{x})$ = dimensionless Gibbs energy of mixing of a mixture at composition $\mathbf{x}$
$\hat{\imath}$ = unit vector representing the direction along x_1 in the ternary phase diagram
$\hat{\jmath}$ = unit vector representing the direction along x_2 in the ternary phase diagram
k_{ij} = binary interaction parameter
n = number of components in the mixture
P = pressure
T = temperature
$v(\mathbf{x})$ = molar volume of a mixture at composition $\mathbf{x}$
v_i = molar volume of pure component i
$\mathbf{x}$ = composition vector
x_i = mole/weight fraction of component i
x_i^S = mole/weight fraction of component i of the stationary point of D
x_1^α/x_1^β = mole/weight fraction of component 1 in phase α/β
$\mathbf{z}$ = composition vector of the feed
z_i = mole/weight fraction of component i in the feed
$Z(\mathbf{x})$ = compressibility factor of a mixture at composition $\mathbf{x}$
Z_i = compressibility factor of pure component i

Literature Cited

(1) Lucia, A.; Padmanabhan, L.; Venkataraman, S. Multiphase equilibrium flash calculations. *Comput. Chem. Eng.* **2000**, *24*, 2557.

(2) Tan, S. P.; Radosz, M. Constructing Binary and Ternary Phase Diagrams on the Basis of Phase Stability Analysis. *Ind. Eng. Chem. Res.* **2002**, *41*, 3722.

(3) Baker, L. E.; Pierce, A. C.; Luks, K. D. Gibbs Energy Analysis of Phase Equilibria. *Soc. Pet. Eng. J.* **1982**, *22*, 731.

(4) Hua, J. Z.; Brennecke, J. F.; Stadtherr, M. A. Enhanced Interval Analysis for Phase Stability: Cubic Equation of State Models. *Ind. Eng. Chem. Res.* **1998**, *37*, 1519.

(5) Tessier, S. R.; Brennecke, J. F.; Stadtherr, M. A. Reliable Phase Stability Analysis for Excess Gibbs Energy Models. *Chem. Eng. Sci.* **2000**, *55*, 1785.

(6) Xu, G.; Brennecke, J. F.; Stadtherr, M. A. Reliable Computation of Phase Stability and Equilibrium from the SAFT Equation of State. *Ind. Eng. Chem. Res.* **2002**, *41*, 938.

(7) Kearfott, R. B. *Rigorous Global Search: Continuous Problems*; Kluwer Academic Publishers: Dordrecht, The Netherlands, 1996.

(8) Michelsen, M. L. The Isothermal Flash Problem. Part I. Stability. *Fluid Phase Equilib.* **1982**, *9*, 1.

(9) Wasylkiewicz, S. K.; Sridhar, L. N.; Doherty, M. F.; Malone, M. F. Global Stability Analysis and Calculation of Liquid−Liquid Equilibrium in Multicomponent Mixtures. *Ind. Eng. Chem. Res.* **1996**, *35*, 1395.

(10) Sun, A. C.; Seider, W. D. Homotopy-continuation for the stability analysis in global minimization of the Gibbs free energy. *Fluid Phase Equilib.* **1995**, *103*, 213.

(11) Nichita, D. V.; Gomez, S.; Luna, E. Phase stability analysis with cubic equations of state by using a global optimization method. *Fluid Phase Equilib.* **2002**, *194*−*197*, 411.

(12) Chan, A.; Adidharma, H.; Radosz, M. Fluid−Liquid Transitions of Poly(ethylene-*co*-octene-1) in Supercritical Ethylene Solutions. *Ind. Eng. Chem. Res.* **2000**, *39*, 4370.

(13) Luszczyk, M.; Radosz, M. Temperature- and Pressure-Induced Crystallization and Melting of Tetracontane in Propane. *J. Chem. Eng. Data* **2002**, submitted for publication.

(14) Blas, F. J.; Vega, L. F. Prediction of Binary and Ternary Diagrams Using the Statistical Associating Fluid Theory (SAFT) Equation of State. *Ind. Eng. Chem. Res.* **1998**, *37*, 660.

(15) Huang, S. H.; Radosz, M. Equation of State for Small, Large, Polydisperse, and Associating Molecules. *Ind. Eng. Chem. Res.* **1990**, *29*, 2284.

(16) Huang, S. H.; Radosz, M. Equation of State for Small, Large, Polydisperse, and Associating Molecules: Extension to Fluid Mixtures. *Ind. Eng. Chem. Res.* **1991**, *30*, 1994.

(17) Chan, A.; Hemmingsen, P. V.; Radosz, M. Fluid−Liquid and Fluid−Solid Transitions of Tetracontane in Propane. *J. Chem. Eng. Data* **2000**, *45*, 362.

(18) Press, W. H.; Teukolsky, S. A.; Vetterling, W. T.; Flannery, B. P. *Numerical Recipes in FORTRAN: The Art of Scientific Computing*, 2nd ed.; Cambridge University Press: Cambridge, U.K., 1992.

Received for review June 10, 2002
Revised manuscript received August 9, 2002
Accepted August 13, 2002

IE020430T